

# Calcium aluminates hydration in presence of amorphous SiO<sub>2</sub> at temperatures below 90 °C

J.M. Rivas Mercury<sup>a,1</sup>, X. Turrillas<sup>b,2</sup>, A.H. de Aza<sup>a,\*</sup>, P. Pena<sup>a</sup>

<sup>a</sup>*Instituto de Cerámica y Vidrio, C.S.I.C., Campus de Cantoblanco, C/Kelsen no. 5, 28049 Madrid, Spain*

<sup>b</sup>*Eduardo Torroja for Construction Sciences, C.S.I.C., C/Serrano Galvache no. 4, 28032 Madrid, Spain*

Received 17 March 2006; received in revised form 12 May 2006; accepted 16 May 2006

Available online 2 June 2006

## Abstract

The hydration behaviour of Ca<sub>3</sub>Al<sub>2</sub>O<sub>6</sub>, Ca<sub>12</sub>Al<sub>14</sub>O<sub>33</sub> and CaAl<sub>2</sub>O<sub>4</sub> with added amorphous silica at 40, 65 and 90 °C has been studied for periods ranging from 1 to 31 days. In hydrated samples crystalline phases like katoite (Ca<sub>3</sub>Al<sub>2</sub>(SiO<sub>4</sub>)<sub>3-x</sub>(OH)<sub>4x</sub>) and gibbsite, Al(OH)<sub>3</sub>, were identified, likewise amorphous phases like Al(OH)<sub>x</sub>, calcium silicate hydrates, C–S–H, and calcium aluminosilicate hydrates, C–S–A–H, were identified. The stoichiometry of Ca<sub>3</sub>Al<sub>2</sub>(SiO<sub>4</sub>)<sub>3-x</sub>(OH)<sub>4x</sub> (0 ≤ 3–x ≤ 0.334), which was the main crystalline product, was established by Rietveld refinement of X-ray and neutron diffraction data and by transmission electron microscopy.

© 2006 Elsevier Inc. All rights reserved.

**Keywords:** Calcium aluminates hydration; Katoite; Microsilica; Refractory castables

## 1. Introduction

Modern technology of refractories is of strategic interest in a number of high-temperature industrial processes. More particularly, unshaped monolithic refractories with low cement additions based on alumina raw materials are used ubiquitously in a range of furnace lining applications such as metallurgy, glass foundries, ceramics, petrochemistry, and clinker production to name just a few.

Industrial refractory castables are composed of a fine fraction, or matrix, and an aggregate or coarse component. Novel slip cast refractory materials are formulated with very low additions of calcium aluminate cements and variable additions of active rheological agents such as amorphous microspheres of silica (microsilica<sup>®</sup>; term introduced by Elkem A/S for the material obtained after cleaning, classifying, and homogenising the silica-rich fume

released during production of ferrosilicon and silicon metal in electric arc furnaces [1]), activated alumina and other small grain size additives [1–3].

It has been shown that the main role of microsilica<sup>®</sup> is to fill void spaces between large particles so that the densest possible packing is achieved. On the other hand, it has been demonstrated that the amorphous microspheres of silica enhances the rheological properties of these materials [1–4].

The critical issue of hydration of refractory calcium aluminate cements with microsilica<sup>®</sup>, in the temperature range 40–100 °C, is one of the main challenges in the castable refractory concretes field. However, is not yet fully understood. Indeed the few studies related to this topic indicate that silica reacts with the calcium aluminate phases in the cement and water to form different crystalline hydrates (with variable proportions of Ca, Al, Si) such as Ca<sub>2</sub>Al<sub>2</sub>SiO<sub>7</sub>·8H<sub>2</sub>O [4,5] (strätlingite), Ca<sub>3</sub>Al<sub>2</sub>(SiO<sub>4</sub>)<sub>3-x</sub>(OH)<sub>4x</sub> (0 < x < 3) [6,7] (katoite) and not very well defined and complex zeolite-type phases [8]. Likewise, the presence, between 25 and 85 °C, of non-crystalline and metastable phases, mainly calcium silicate hydrates C–S–H, have been reported by Silva et al. [9] and Damidot et al. [10]. On the other hand, the extent of Si substitution in the stable hydrogarnet, katoite, has not yet been quantified.

\*Corresponding author. Fax: +34 91 735 58 43.

E-mail address: [aaza@icv.csic.es](mailto:aaza@icv.csic.es) (A.H. de Aza).

<sup>1</sup>Permanent address: Centro Federal de Educação Tecnológica do Maranhão—CEFET-MA Av. Getúlio Vargas, 04-Monte Castelo—CEP 65025-001—São Luís-MA—Brasil.

<sup>2</sup>Current address: ESRF (European Synchrotron Radiation Facility), 6 rue Jules Horowitz, BP220, 38043 Grenoble Cedex, France.

Having that in mind,  $\text{Ca}(\text{OH})_2$ ,  $\text{Al}(\text{OH})_3$ ,  $\text{CaAl}_2\text{O}_4 \cdot 10\text{H}_2\text{O}$ ,  $\text{Ca}_2\text{Al}_2\text{O}_5 \cdot 8\text{H}_2\text{O}$ ,  $\text{Ca}_2\text{Al}_2\text{SiO}_7 \cdot 8\text{H}_2\text{O}$  and a series of solid solutions, of general formula  $\text{Ca}_3\text{Al}_2(\text{SiO}_4)_{3-x}(\text{OH})_{4x}$ , can be located in the  $\text{CaO}-\text{Al}_2\text{O}_3-\text{SiO}_2-\text{H}_2\text{O}$  system for temperatures below  $100^\circ\text{C}$ . Indeed, the whole series exists with the end members known as grossular for  $x = 0$  and hydrogarnet for  $x = 3$ . Since the solution series occurs in nature, mineralogists classify them as hibschite for the minerals with  $0.2 < x < 1.5$  and as katoite for the ones with  $1.5 < x < 3$ . Different authors synthesised these compounds at temperatures lower than  $350^\circ\text{C}$  in a hydrothermal environment and they characterized the obtained phases by XRD, ND and IR spectroscopy analysis, respectively [6,11]. Within the same system, some other crystalline hydrates co-exist with the former solid solutions. They appear in Portland cements and in hydrothermal activated metakaolin (calcium hydroxide systems) as reported by Silva and Glasser [9] and Jappy and Glasser [7]. Also, the persistence of non-crystalline hydrates particularly the above mentioned C–S–H and calcium aluminosilicate hydrates, C–S–A–H, and the formation of crystalline  $\text{Ca}_2\text{Al}_2\text{SiO}_7 \cdot 8\text{H}_2\text{O}$  between 25 and  $85^\circ\text{C}$  have been reported [9,10].

The present contribution has been focused to the hydration reaction progress of  $\text{Ca}_3\text{Al}_2\text{O}_6$ ,  $\text{Ca}_{12}\text{Al}_{14}\text{O}_{33}$  and  $\text{CaAl}_2\text{O}_4$  in the presence of microsilica<sup>®</sup>. The hydration behaviour of calcium aluminates and amorphous silica mixtures have been investigated at 40, 65 and  $90^\circ\text{C}$  by X-ray diffraction (XRD), neutron diffraction (ND) and transmission electron microscopy fitted with energy dispersive X-ray analyser (TEM-EDS). The diffraction data treatment has allowed a quantification of silicon substitution in the katoite series and from the global interpretation of the results it has been possible to establish the development and stability relations of hydrates.

## 2. Experimental

### 2.1. Synthesis

Details of the mechanochemical method used for the synthesis of the calcium aluminates are given elsewhere [12,13]. Eleven different compositions were selected along the  $\text{Ca}_3\text{Al}_2\text{O}_6-\text{SiO}_2$ ,  $\text{Ca}_{12}\text{Al}_{14}\text{O}_{33}-\text{SiO}_2$  and  $\text{CaAl}_2\text{O}_4-\text{SiO}_2$  composition lines drawn to cover both low, and high,  $\text{SiO}_2$  regions. The molar ratios of the compositions are shown in Table 1.

The specimens examined were obtained through deutero-hydration (with  $\text{D}_2\text{O}$  99.9% from Merck; Darmstadt, Germany) of pure synthetic polycrystalline  $\text{Ca}_3\text{Al}_2\text{O}_6$ ,  $\text{Ca}_{12}\text{Al}_{14}\text{O}_{33}$  and  $\text{CaAl}_2\text{O}_4$  and amorphous silica (Elken microsilica<sup>®</sup> 983; Elken Materials, Inc., Pittsburg, PA >98% reactive  $\text{SiO}_2$ ,  $0.15\ \mu\text{m}$  amorphous microspheres) powder mixtures. The chemical analysis and physical properties of the solid precursor phases are listed in Table 2. The specimens were treated with  $\text{D}_2\text{O}$  in an attempt to substitute the hydrogen by deuterium in the hydrates formed. The reason for that is that neutrons interact with hydrogen atoms producing an incoherent scattering in all directions, manifested by a notable increase of background in diffraction patterns. Nevertheless, it is difficult to achieve complete replacement of  $\text{H}_2\text{O}$  by  $\text{D}_2\text{O}$ . In most of the cases a fraction is replaced, hence a significant background is usually recorded. Also, it has to be noted that hydrogen and deuterium are indistinguishable from a chemical point of view and that they occupy the same crystallographic sites forming a complete hydrogen–deuterium “solid solution”. Therefore, the different partially deuterated species were written as if only hydrogen atoms were present. The reported  $\text{H}_2\text{O}/\text{D}_2\text{O}$  ratio value was established by Rietveld refinement using both XRD and ND data.

Table 1  
Calcium aluminates-silica compositions selected

Ref.	Composition	Composition (mol%)		
		CaO	$\text{AlO}_{1.5}$	$\text{SiO}_2$
1.5	$\text{CaAl}_2\text{O}_4 + 5.26\text{SiO}_2$	12.1	24.2	63.1
1.4	$\text{CaAl}_2\text{O}_4 + 2.63\text{SiO}_2$	17.7	35.5	46.8
1.3	$\text{CaAl}_2\text{O}_4 + 2.4\text{SiO}_2$	26.2	52.7	21.1
1.2	$\text{CaAl}_2\text{O}_4 + 1.7\text{SiO}_2$	28.9	56.1	15.9
1.1	$\text{CaAl}_2\text{O}_4 + 0.4\text{SiO}_2$	31.7	64.0	4.3
1.0	$\text{CaAl}_2\text{O}_4$	33.2	66.8	0.0
2.3	$\text{Ca}_{12}\text{Al}_{14}\text{O}_{33} + 2.4\text{SiO}_2$	33.7	39.2	27.1
2.2	$\text{Ca}_{12}\text{Al}_{14}\text{O}_{33} + 1.7\text{SiO}_2$	36.6	42.6	28.8
2.1	$\text{Ca}_{12}\text{Al}_{14}\text{O}_{33} + 0.4\text{SiO}_2$	43.5	50.7	5.8
2.0	$\text{Ca}_{12}\text{Al}_{14}\text{O}_{33}$	46.1	53.9	0.0
3.3	$\text{Ca}_3\text{Al}_2\text{O}_6 + 2.4\text{SiO}_2$	40.5	27.0	32.5
3.2	$\text{Ca}_3\text{Al}_2\text{O}_6 + 1.7\text{SiO}_2$	44.8	39.8	25.4
3.1	$\text{Ca}_3\text{Al}_2\text{O}_6 + 0.4\text{SiO}_2$	55.6	37.0	7.4
3.0	$\text{Ca}_3\text{Al}_2\text{O}_6$	60.0	40.0	0.0

Table 2  
Chemical analysis of the synthetic raw materials used

	CaAl <sub>2</sub> O <sub>4</sub>	Ca <sub>12</sub> Al <sub>14</sub> O <sub>33</sub>	Ca <sub>3</sub> Al <sub>2</sub> O <sub>6</sub>	Microsilica <sup>®</sup>
<i>Chemical analysis</i>				
CaO	35.1	51.8	62.3	0.2
Al <sub>2</sub> O <sub>3</sub>	64.6	48.0	37.4	0.2
Na <sub>2</sub> O	0.1	0.1	0.1	0.04
SiO <sub>2</sub>	0.1	0.1	0.2	98.3
Grain size <i>D</i> <sub>50</sub> (μm)	5.7	3.5	2.7	≈ 150 nm <sup>a</sup>
Specific surface (m <sup>2</sup> /g)	1.2			17.0
Real density (g/cm <sup>3</sup> )	2.9	2.5	2.8	2.27

<sup>a</sup>Measured by TEM.

Microsilica<sup>®</sup>-calcium aluminate samples were mixed with excess of D<sub>2</sub>O in a ratio of heavy water/solids = 2, and placed in a teflon recipient, that could be kept tightly closed with a lid and an o-ring, at 40, 65 and 90 °C for several hours. The deuterio-hydrated pastes were milled and sieved (120 μm) treated once more with D<sub>2</sub>O in a closed vessel at the same temperatures and homogenised every 24 h. This process was repeated several times to complete 7 days at 40 and 65 °C and 31 days at 90 °C to get homogeneous powders under 120 μm. The resulting powders were analysed by XRD and consisted of gibbsite [14] and/or hydrogarnet [15] (gibbsite, hydrogarnet and katoite powder diffraction files: 33-0018, 84-1354 and 38-0368 ICDD 2000 and ICSD, database).

The experiments were conducted by mixing the amorphous silica with calcium aluminates in water because the other components present in real refractory castables (although important from a mechanical point of view) are chemically inactive at temperatures lower than ~800 °C. Therefore, the coarse particles of castables were not added for two main reasons: their chemical activity in the hydration process is negligible and they would interfere in the characterisation by diffraction techniques and TEM.

## 2.2. Diffraction studies

### 2.2.1. X-ray

A Kristalloflex 710 D5000 (Siemens, Germany) diffractometer (Bragg–Brentano geometry) was used for phase analysis by XRD. Powder diffraction patterns were recorded using CuK $\alpha_{1,2}$  radiation (1.5418 Å) with a secondary curved graphite monochromator. The X-ray tube operated at 40 kV and 30 mA. For the routine analysis of phase identification an angular window from 2° to 70° 2 $\theta$  was scanned with a step size 0.05° 2 $\theta$  and a time of 5 s/step. The samples were rotated at 15 rpm during acquisition to minimise orientation effects of diffraction peaks.

For Rietveld analysis, the diffraction data were acquired between 10° and 130° in 2 $\theta$  in two sets: from 10° to 90° (2 $\theta$ ) with sample rotation at 15 r.p.m and from 90 to 130 without rotation. Both sets were acquired with a step size of 0.03° and 20 s/step. The pre-sample slit used was 2 mm

wide and for the detector three slits of 2, 0.2 and 0.6 were set.

As very precise positions of diffraction peaks were necessary silicon powder from NIST (reference material SRM Si-640b,  $a = 5.430940$  Å, National Institute for Standards and Technology, Gaithersburg, MD) was used as an internal standard for  $d$ -spacings [16]. The powder was added to the powder specimens in a proportion of 20% by weight.

### 2.2.2. Neutrons

The powder ND experiments were carried out at the Swiss Spallation Neutron Source (SINQ) of Paul Scherrer Institut (PSI) in Villigen, Switzerland [17]. The instrument HRPT [18] in high-intensity mode was employed with  $\lambda = 1.8857$  Å in the angular range from 2.45° to 163° 2 $\theta$  with an equivalent step size of 0.05°. The patterns were collected to accumulate 10<sup>6</sup> monitor counts. Approximately, 5 g of well-compacted polycrystalline powder was introduced into a cylindrical stainless steel tube of 10 mm internal diameter and 60 mm long. The cylinder was closed with a security lid that allowed releasing of water pressure.

### 2.2.3. Data treatment

Powder diffraction patterns were analysed by Rietveld, using FULLPROF [19]. General plotting and fitting of data was done with the help of Origin [20] v6.

### 2.2.4. Rietveld refinements

The refinements were carried out in a conventional way following the strategy and recommendations of McCusker et al. [21] by using a pseudo-Voigt peak shape function with the asymmetry correction of Finger et al. [22] included when needed. The optimised parameters were: background coefficients, zero-shift error (using an internal standard of silicon powder from NIST as mentioned above), peak shape parameters (including anisotropic terms when appropriate), cell parameters and silicon substitution. Here, it is worth to mention that there is a linear dependence between the cell lattice parameter of katoite and the amount of silicon substituted in the crystal structure. This linear relationship was obtained by plotting the data published by different authors [6,15,23–26]

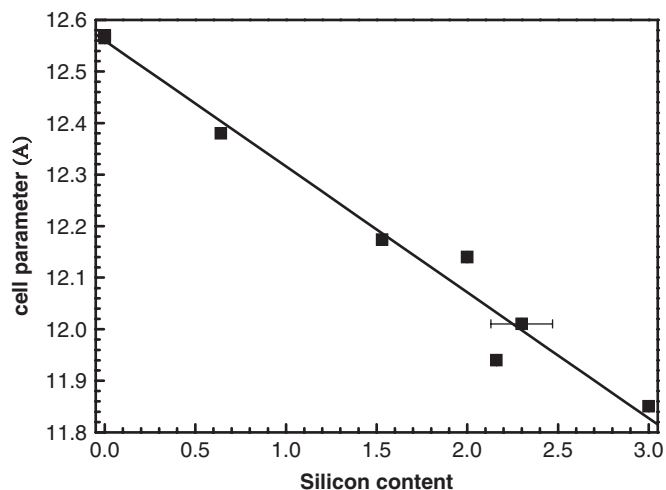


Fig. 1. Linear dependence between the cell lattice parameter of katoite and the amount of silicon substituted in the crystal structure:  $\text{Ca}_3\text{Al}_2(\text{SiO}_4)_{3-x}(\text{OH})_{4x}$  ( $x = 0-3$ ).

gathered in the Inorganic Crystal Structure Database [27] and fitting them to a straight line [15,28], Fig. 1. This linear relationship was introduced as a constraint during the Rietveld refinements. Also, a second constraint for the hydrogen population since it depends on the amount of silicon present in the formula [15] was introduced.

When ND data were available, both X-ray and neutron sets of data were used for simultaneous refinement. In this case, it was possible to refine the populations of hydrogen and deuterium.

Examples of some of the Rietveld refinements can be seen in Figs. 2a and b. The values of the pattern-dependent,  $R_{\text{WP}}$ , disagreement factor [29–31], and the values of the phase-dependent,  $R_{\text{F}}$ , disagreement factor [29–31] were evaluated and they are listed in Table 3 together with the statistical reliability factor of Bragg,  $R_{\text{B}}$  [29]. The values listed indicate that fits are satisfactory.

### 2.3. Microstructural studies

Microstructural analyses and phase identification were done by TEM (Hitachi-H7100 (Japan) at 125 kV, fitted with EDS analyser (Rentec-M-series, Germany) with an acquisition time of 300 s. Powdered samples were dispersed in propan-2-ol and mounted on carbon-coated copper grids.

## 3. Results

### 3.1. Hydration progress monitored by XRD

The evolution of hydration with  $\text{D}_2\text{O}$  for the different mixtures as a function of time and temperature was followed by XRD. The results are gathered in Tables 4–6 for 40, 65 and for 90 °C, respectively. In all cases, the heavy water/solids ratio was 2 by weight. The crystal phases found after the treatments were unreacted

calcium aluminates (at 40 °C only),  $\text{Ca}_2\text{Al}_2\text{O}_5 \cdot 8\text{H}_2\text{O}$ ,  $\text{Ca}_3\text{Al}_2(\text{OH})_{12}$ , and  $\text{Al}(\text{OH})_3$  ( $\text{Ca}_2\text{Al}_2\text{O}_5 \cdot 8\text{H}_2\text{O}$  Powder Diffraction File: 45–0564 ICDD 2000 and ICSD data base).

The amount of amorphous phases was roughly estimated in a qualitative way from the background of the XRD patterns of each sample. Another sign of the low crystallinity of samples was the low intensity of diffraction peaks in the XRD patterns.

As expected, the hydration rate of all the samples increased with temperature. Only at 40 °C and during the earlier days the metastable  $\text{Ca}_2\text{Al}_2\text{O}_5 \cdot 8\text{H}_2\text{O}$  was detected. In all cases at the end, katoite and amorphous phases were found. Additionally, for  $\text{CaAl}_2\text{O}_4$  and  $\text{Ca}_{12}\text{Al}_{14}\text{O}_{33}$  mixtures gibbsite was also detected. Another trend observed was the increase of amorphous phases for the specimens with higher content of amorphous silica. In the samples with higher silica content the formation of  $\text{Ca}_2\text{Al}_2\text{SiO}_7 \cdot 8\text{H}_2\text{O}$  (ICDD card #29-0285) was observed at 65 °C.

### 3.2. Rietveld refinements

Following the strategy described previously the stable hydrate, namely katoite, was refined. The results obtained are shown in Table 3. In all cases, katoite single phases with varying cell parameters were observed, i.e. no splitting of the diffraction peaks occurred. Rietveld plots for some analysed samples with the observed, calculated and difference powder patterns are shown in Figs. 2a and b.

### 3.3. Electron microscopy study

Figs. 3 and 4 show typical TEM images of some hydrated samples. After close examination, faceted grey crystals of  $\text{Ca}_3\text{Al}_2(\text{OH})_{12}$  can be identified. In general, Si-containing samples show a homogenous microstructure. The TEM micrographs show randomly distributed agglomerates of un-reacted microsilica<sup>®</sup> particles (50–150 nm), see Fig. 3, and cubic crystals of katoite having a composition of  $\text{Ca}_3\text{Al}_2(\text{SiO}_4)_{3-x}(\text{OH})_{4x}$  ( $0 \leq 3-x \leq 0.5$ ) (Figs. 3 and 4). In  $\text{Ca}_{12}\text{Al}_{14}\text{O}_{33}$ /silica and  $\text{CaAl}_2\text{O}_4$ /silica mixtures,  $\text{Al}(\text{OH})_3$ , gibbsite, crystals were additionally detected (Fig. 4).

As mentioned previously, composition of the spherical amorphous phases and the crystalline hydrogarnets of each formulation were determined by TEM-EDS. Average results of 10 measurements of katoite phase composition is given in Table 7.

## 4. Discussion

### 4.1. Evolution of phases with temperature

During the hydration of selected mixtures, at temperatures varying from 40° to 90°, the crystalline phases that precipitated were the expected according to the current knowledge on the subject.

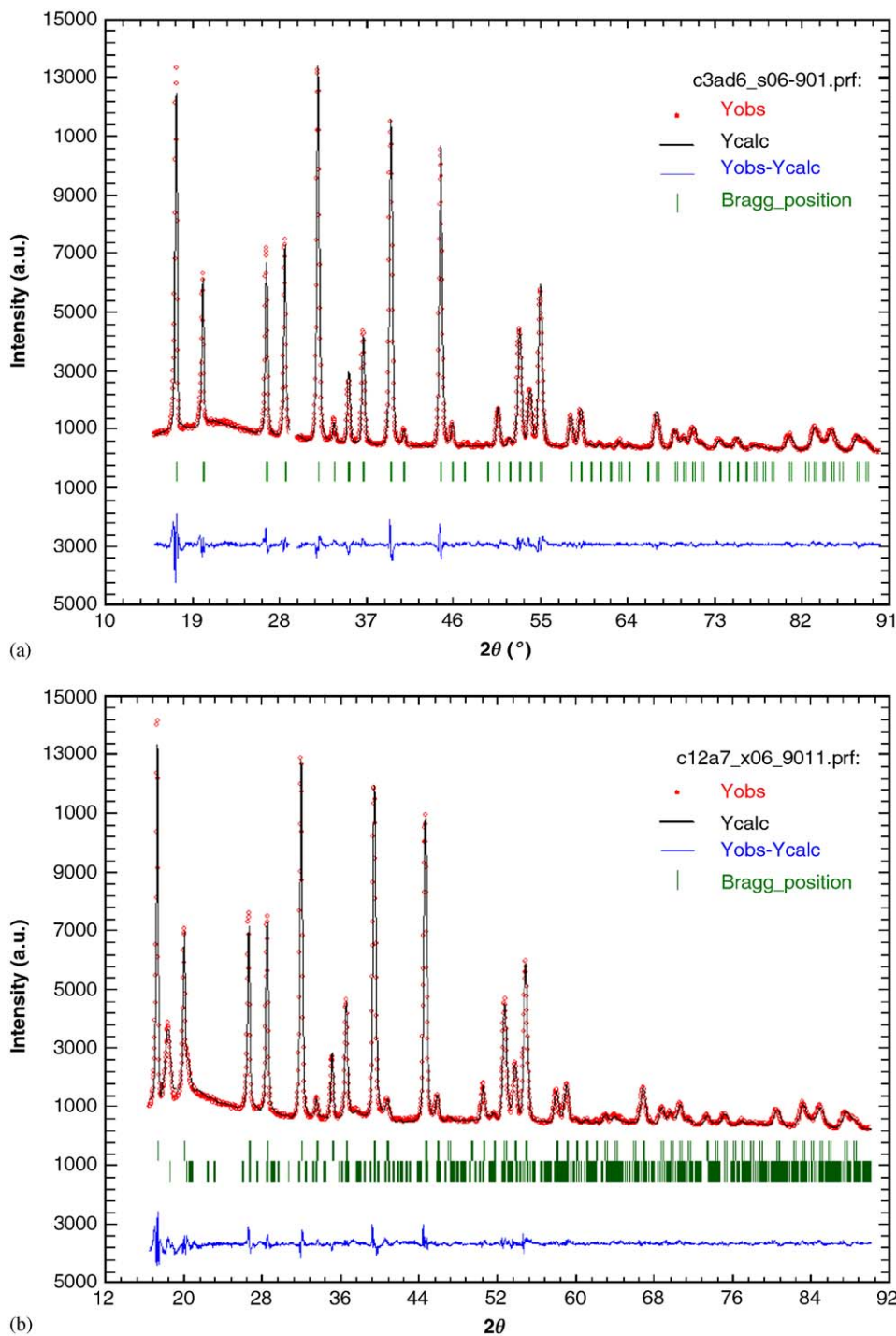


Fig. 2. Rietveld plots (for some analysed compositions hydrated 31 days at 90 °C) with the observed calculated and difference powder patterns: (a) Rietveld analysis of 3.3 sample. According to the obtained data it is composed of katoite:  $\text{Ca}_3\text{Al}_2\text{Si}_{0.33}(\text{OH})_{10.70}$ . (b) Rietveld analyses of 2.3 sample. According to the obtained data it is composed of: 83 wt% katoite ( $\text{Ca}_3\text{Al}_2(\text{SiO}_4)_{0.25}(\text{OH})_{11}$ ) and 17 wt% of gibbsite ( $\text{Al}(\text{OH})_3$ ). The relative amount of katoite and gibbsite corresponded to the expected from the stoichiometry of the reaction involved.

These observations could be summarised by saying that in the early stages and at lower temperatures, metastable hydrates such as  $\text{Ca}_2\text{Al}_2\text{O}_5 \cdot 8\text{H}_2\text{O}$  precipitated. As time progressed they gave way to the stable phases, i.e.  $\text{Ca}_3\text{Al}_2(\text{OH})_{12}$  (katoite) and  $\text{Al}(\text{OH})_3$  (gibbsite). It is well known that this process is faster at higher temperatures [32] or when it happens under a moist closed atmosphere. Their

formation under these particular conditions with a water/solids ratio of 2 and 40–90 °C occurs through a solution-precipitation process of thermodynamically stable phases.

The hydration process occurs with the dissolution of the anhydrous phase and is followed by the precipitation of the thermodynamically stable hydrates. Three distinct steps can be identified: dissolution, nucleation and precipitation. The

Table 3  
XRD and ND Rietveld refinement results

Sample	$T/t$ (°C/day)	Red parameter (Å)	$R_{wp}$	$R_B$	$R_F$	Si substitution	$H+D^a$	$H^b$	$D^b$
1.3	90/31	$12.525 \pm 0.003$	11.40	5.40	3.32	$0.19 \pm 0.01$	$11.24 \pm 0.04$	—	—
2.1	65/7	$12.546 \pm 0.001^b$	11.50	11.00	9.5	$0.11 \pm 0.01$	11.56	2.67	8.89
2.3	65/7	$12.554 \pm 0.002$	11.00	3.74	2.66	$0.08 \pm 0.01$	$11.67 \pm 0.04$	—	—
2.3	90/31	$12.512 \pm 0.002$	5.77	1.25	1.07	$0.25 \pm 0.01$	$11.02 \pm 0.04$	—	—
3.0	65/7	$12.575 \pm 0.001^b$	2.99	9.07	6.43	Undetected	12	5.88	6.12
3.1	40/7	$12.563 \pm 0.001^b$	10.40	5.84	4.78	$0.04 \pm 0.01$	11.94	0.14	11.8
3.3	40/7	$12.547 \pm 0.001$	8.43	3.69	2.60	$0.10 \pm 0.01$	$11.61 \pm 0.04$	—	—
3.2	65/7	$12.528 \pm 0.001$	8.15	2.25	1.50	$0.18 \pm 0.01$	$11.24 \pm 0.04$	—	—
3.3	65/7	$12.529 \pm 0.001$	8.64	2.36	2.94	$0.18 \pm 0.01$	$11.30 \pm 0.04$	—	—
3.3	90/31	$12.495 \pm 0.002$	9.79	1.78	1.22	$0.33 \pm 0.02$	$10.69 \pm 0.51$	—	—

$R_{wp}$ : pattern-dependent disagreement factor [30–32],  $R_F$ : phase-dependent disagreement factor [30–32] and  $R_B$ : statistical reliability factor of Bragg [30].

<sup>a</sup>Data obtained by XRD Rietveld refinement.

<sup>b</sup>Data obtained by XRD and ND simultaneous Rietveld refinement.

Table 4  
Hydration progress with time on hydrated samples at 40 °C. XRD results

Ref.	Time	Hydrated phases by XRD					
		$Ca_3Al_2(OH)_{12}$	$Ca_3Al_2(SiO_4)_{3-x}(OH)_{4x}$	$Al(OH)_3$	$Ca_2Al_2O_5 \cdot 8H_2O$	Amorphous phase	Calcium aluminate
1.3	1 day	—	+	+	++	—	+
	2 days	—	+	+	+++	+	+
	3 days	—	++	++	+	+	—
	7 days	—	+++	++	—	+	—
1.2	1 day	—	+	+	+++	+	+
	2 days	—	++	+	++	+	—
	3 days	—	++	++	+	+	—
1.1	1 day	—	+	+	++	+	+
	2 days	—	++	++	+++	+	+
	3 days	—	+++	++	+	+	—
1.0	1 day	—	—	+	+	—	+
	3 days	++	—	++	—	+	+
	7 days	+++	—	++	—	+	+
3.3	1 h	—	+++	—	—	—	—
	1 day	—	+++	—	—	—	—
	7 days	—	+++	—	—	—	—
3.2	1 h	—	+++	—	—	—	—
	1 day	—	+++	—	—	—	—
	7 days	—	+++	—	—	—	—
3.1	1 day	—	+++	—	—	+	—
	7 days	—	+++	—	—	+	—
3.0	1 h	+++	—	—	—	—	—
	1 day	+++	—	—	—	—	—
	7 days	+++	—	—	—	—	—

Water/solids ratio = 2 by weight (solids = calcium aluminate + silica), h = hours.

—: absent phase; +: identified phase; ++: abundant phase; +++: very abundant phase.

hydration process is initiated by the hydroxylation of the calcium aluminate surface followed by dissolution of Ca in water and the formation of  $Ca^{2+}$  and  $AlO_2^-$  species. A small amount of hydrates will precipitate at this point if the solution concentration reaches and trespasses the solubility product of the hydrates  $Ca_2Al_2O_5 \cdot 8H_2O$  and  $Al(OH)_3$  [1,2].

Jensen et al. [33] and Christensen et al. [34] have been studied *in situ* by synchrotron X-ray powder diffraction, in the temperature range 25–170 °C, the hydrothermal trans-

formation of  $CaAl_2O_4 \cdot 10H_2O$  and  $Ca_2Al_2O_5 \cdot 8H_2O$  to  $Ca_3Al_2(OH)_{12}$  and  $Al(OH)_3$ . They were able to detect a very elusive transient phase such as  $Ca_4Al_2O_7 \cdot 19H_2O$ . During the experiments described in the present investigation this intermediate phase, detected in the first stage of the hydration for pure calcium aluminate by the mentioned authors, was not detected. This can be explained because the resolution of the data acquisition did not permit to spot those transient hydrates.

Table 5  
Hydration progress with time on hydrated samples at 65 °C. XRD results

Ref.	Time (days)	Hydrated phases identified by XRD			
		$\text{Ca}_3\text{Al}_2(\text{OH})_{12}$	$\text{Ca}_3\text{Al}_2(\text{SiO}_4)_{3-x}(\text{OH})_{4x}$	$\text{Ca}_2\text{Al}_2\text{SiO}_7 \cdot 8\text{H}_2\text{O}$	$\text{Al}(\text{OH})_3$
1.5	1	–	+	–	+
	7	–	++	+	+
	15	–	++	+?	+
1.4	3	–	+++	+?	++
	7	–	+++	–	+++
1.3	7	–	+++	–	++
1.2	7	–	+++	–	++
1.0	1	+++	–	–	++
	7	+++	–	–	++
2.3	7	–	+++	–	+
2.2	7	–	+++	–	+
2.0	7	+++	–	–	+
3.3	7	–	+++	–	–
3.2	7	–	+++	–	–
3.0	7	+++	–	–	–

Water/solids ratio = 2 by weight (solids = calcium aluminate + silica).

–: absent phase; +: identified phase; ++: abundant phase; +++: very abundant phase.

Table 6  
XRD identified hydrates

Ref.	Hydrated phases identified by XRD (wt%)		
	$\text{Ca}_3\text{Al}_2(\text{OH})_{12}$	$\text{Ca}_3\text{Al}_2(\text{SiO}_4)_{3-x}(\text{OH})_{4x}$	$\text{Al}(\text{OH})_3$
1.3	–	+++	+++
2.3	–	+++	++
3.3	–	+++	–
3.0	+++	–	–

The samples were hydrated up to 31 days at 90 °C, but the identified phases do not change from 1 up to 31 days.

Water/solids ratio = 2 by weight (solids = calcium aluminate + silica).

–: absent phase; +: identified phase; ++: abundant phase; +++: very abundant phase.

Table 7  
Analytical transmission electron microscopic data obtained on selected hydrated mixtures

Ref.	T/time (°C/day)	Phases identified by TEM-EDS		
		Katoite microanalysis	Amorphous $\text{SiO}_2$	Gibbsite $\text{Al}(\text{OH})_3$
3.1	40/7	$\text{Ca}_{3.0 \pm 0.2}\text{Al}_{2.3 \pm 0.2}(\text{SiO}_4)_{0.04 \pm 0.02}(\text{OH})_{11.84}$	$\text{SiO}_2$	Undetected
3.2	65/7	$\text{Ca}_{3.0 \pm 0.2}\text{Al}_{2.3 \pm 0.3}(\text{SiO}_4)_{0.2 \pm 0.1}(\text{OH})_{11.2}$	$\text{SiO}_2$	Undetected
3.0	65/7	$\text{Ca}_{3.0 \pm 0.2}\text{Al}_{2.1 \pm 0.1}(\text{OH})_{12}$	Undetected	Undetected
1.3	90/31	$\text{Ca}_{3.0 \pm 0.2}\text{Al}_{2.4 \pm 0.2}(\text{SiO}_4)_{0.5 \pm 0.3}(\text{OH})_{10}$	$\text{SiO}_2$	$\text{Al}(\text{OH})_3$
2.3	90/31	$\text{Ca}_{3.0 \pm 0.2}\text{Al}_{2.4 \pm 0.2}(\text{SiO}_4)_{0.5 \pm 0.2}(\text{OH})_{10}$	$\text{SiO}_2$	$\text{Al}(\text{OH})_3$
3.3	90/31	$\text{Ca}_{3.0 \pm 0.2}\text{Al}_{2.3 \pm 0.1}(\text{SiO}_4)_{0.5 \pm 0.3}(\text{OH})_{10}$	Undetected	Undetected

It is pertinent to mention that in the literature there is not a unanimous agreement about the precipitation of  $\text{Ca}_2\text{Al}_2\text{SiO}_7 \cdot 8\text{H}_2\text{O}$  under these conditions. Some authors reported its existence [3,4], but some others could not find it [1]. In the experiments conducted in the present work ( $w/s = 2$  and 40–90 °C), the crystalline phase  $\text{Ca}_2\text{Al}_2\text{SiO}_7 \cdot 8\text{H}_2\text{O}$  was not detected either by XRD, ND or

TEM in specimens with silica content lower than 22 mol%. The former phase was detected by XRD in specimens with higher silica content (> 50 mol%) and hydrated at 65 °C. This might be due to the low concentration of silicate ions in the aqueous phase. Despite of the concentration increase of silicon species with temperature the concentration of  $\text{SiO}_4^{4-}$  did not reach the solubility product to precipitate

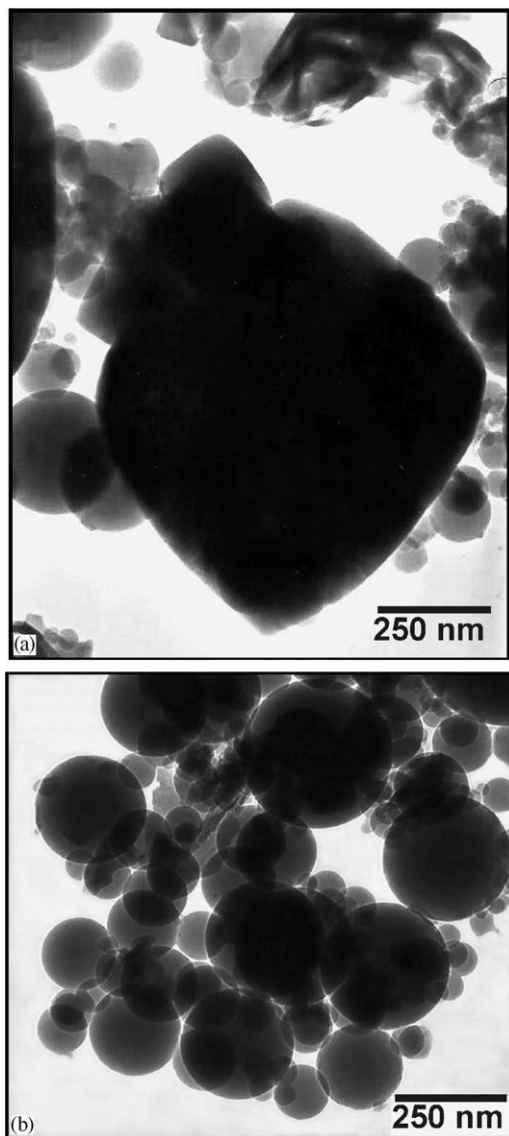


Fig. 3. Typical TEM micrographs of  $\text{Ca}_3\text{Al}_2\text{O}_6 + 1.7\text{SiO}_2$  composition hydrated at  $65^\circ\text{C}$  for 7 days showing cubic,  $\text{Ca}_3\text{Al}_2(\text{SiO}_4)_{3-x}(\text{OH})_{4x}$  ( $0 < x < 3$ ) katoite crystals (a) and un-reacted amorphous silica spheres (b).

$\text{Ca}_2\text{Al}_2\text{SiO}_7 \cdot 8\text{H}_2\text{O}$ , even at  $65^\circ\text{C}$  and after long reaction periods. According to other authors this phase is not stable [1].

Otherwise in experiments made in samples with large amorphous silica additions, ( $\text{CaAl}_2\text{O}_4 + 5.26\text{SiO}_2$ ) with a  $w/s = 0.4$  and 2 at  $65^\circ\text{C}$  and after long hydration times, very small quantities of  $\text{Ca}_2\text{Al}_2\text{SiO}_7 \cdot 8\text{H}_2\text{O}$  could be observed [35].

Regarding the amorphous components, a significant quantity of unreacted spherical particles of amorphous silica coexisting with amorphous calcium aluminosilicate hydrates, C–S–A–H, and  $\text{Al}(\text{OH})_x$  and crystalline phases was observed by TEM in all the samples studied. The persistence of unreacted amorphous silica may be explained if we take into account the very low concentration

of silica in the aqueous phase ( $\sim 0.6 \times 10^{-7}$  mol/L according to Jappy and Glasser [7]).

These reported low concentrations corroborate the previous arguments about the absence of  $\text{Ca}_2\text{Al}_2\text{SiO}_7 \cdot 8\text{H}_2\text{O}$  at high water/solids ratios and temperatures above  $40^\circ\text{C}$ . Additionally, this low solubility of silicate ions in the same temperature interval could explain the low substitution of silicon in the katoite phase [36]  $\text{Ca}_3\text{Al}_2(\text{SiO}_4)_{3-x}(\text{OH})_{4x}$  ( $0 \leq 3-x \leq 0.3$ ).

Finally, it is worth to mention that in all studied samples calcium hydroxide is absent.

#### 4.2. Rietveld analysis of katoite

As it has been explained, the end member of katoite of general formula  $\text{Ca}_3\text{Al}_2(\text{SiO}_4)_{3-x}(\text{OH})_{4x}$  ( $0 < x < 3$ ) is known as hydrogarnet  $\text{Ca}_3\text{Al}_2(\text{OH})_{12}$ . It is a cubic phase with S.G. Ia3d (230),  $a = 12.55695$  (3) Å and  $z = 8$  [15,24,25]. It belongs to the garnet family and it consists of a three-dimensional framework built up of  $[\text{Al}(\text{OH})_6]$  octahedra with  $[\text{Ca}(\text{OH})_8]$  dodecahedra (distorted hexahedra) and empty  $[(\text{OH})_4]$  tetrahedra. As Si enters the crystal structure, a solid solution is formed and empty  $[(\text{OH})_4]$  tetrahedra are replaced by  $[\text{SiO}_4]$  tetrahedral units. This progressive substitution shrinks the crystal framework, since the volume of a  $[\text{SiO}_4]$  tetrahedron is much smaller than an empty  $[(\text{OH})_4]$  tetrahedron, and consequently the cell parameter decreases linearly, following Vegard's Law [37], from 12.565 Å (Lager et al. [15]) for  $\text{Ca}_3\text{Al}_2(\text{OH})_{12}$  to 11.850 Å for  $\text{Ca}_3\text{Al}_2\text{Si}_3\text{O}_{12}$  [6,26]. See Fig. 1. As mentioned previously, this relationship was kept in mind and used as a constraint during the Rietveld analysis.

The refinements were possible because well defined (in terms of crystallinity) solid solutions of katoite were obtained, i.e. no mixture of two or more solid solutions were observed. This is in contrast with the results reported of Jappy and Glasser [7] on hydrates obtained by refluxing mixtures of CaO, basic active alumina and silicic acid with continuous stirring. They obtained hydrated samples with two distinct katoite phases of different silicon content.

Bearing in mind the experimental conditions, the first obvious observation is that very little amounts of silicon enter the crystal structure of katoite, no more than a 10% of the amorphous silica added. This must be related to the low solubility of silicate species in water. In fact it seems that as the temperature increases, the substitution is higher. It could be concluded that the mechanism of substitution is by solution-precipitation.

#### 4.3. Study by TEM-EDS

The silicon substitution in the hydrogarnet inferred from XRD and ND Rietveld analysis (much lower than the expected target one) supports the possibility of amorphous calcium silicate hydrates, C–S–H, and/or calcium aluminosilicate hydrates, C–S–A–H, and  $\text{AH}_x$  phases formation.

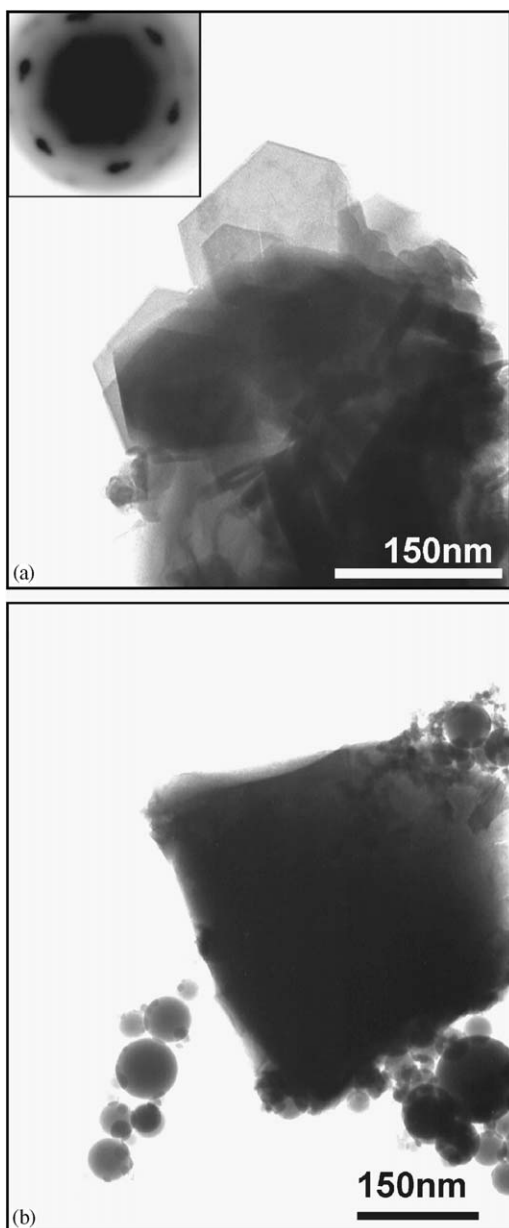


Fig. 4. TEM micrographs of  $\text{CaAl}_2\text{O}_4 + 2.4\text{SiO}_2$  mixture hydrated for 31 days at  $90^\circ\text{C}$  showing gibbsite (a) and cubic katoite ( $\text{Ca}_{3.0 \pm 0.2}\text{Al}_{2.4 \pm 0.2}(\text{SiO}_4)_{0.5 \pm 0.3}(\text{OH})_{10}$ ) crystals with unreacted microsilia spheres (b). Inserted is the selected area electron diffraction (SAED) pattern of gibbsite.

TEM-EDS study shows the presence of cubic katoite grains surrounded by partially reacted amorphous silica spheres. From this type of microstructures it is clear that amorphous silica is not dissolved in water at the experimental conditions used in this study (Figs. 3 and 4).

As it can be seen in Table 7, the elemental composition of katoite phases lay in the range  $\text{Ca}_3\text{Al}_{2.3 \pm 0.2}(\text{SiO}_4)_{0.04 \pm 0.02}(\text{OH})_{11.84} - \text{Ca}_3\text{Al}_{2.3 \pm 0.2}(\text{SiO}_4)_{0.5 \pm 0.3}(\text{OH})_{10}$ , these values show an overestimation of Si content compared with those found by Rietveld analysis. The apparent discrepancies could be explained if the errors of the TEM-EDS technique are taken into account (size of microanalysis area and the

presence of small microsilia<sup>®</sup> particles,  $\sim 150\text{nm}$  around all crystalline phases in the samples). So the discrepancy might be due to the intimate association of microsilia<sup>®</sup> particles and amorphous phases with katoite (Figs. 3 and 4). Additionally, the solid solutions extension established by Rietveld refinement of X-ray and ND data and by TEM-EDS have been recently confirmed by solid state  $^{27}\text{Al}$  and  $^{29}\text{Si}$  NMR [35]. The formation of amorphous calcium aluminosilicate hydrates C–S–A–H was also confirmed by Si NMR.

#### 4.4. Practical implications

Spheres of silica are easily dispersed in the spaces between each cement grain when the refractory castable is freshly mixed. It is quite clear that the primary function of microsilia in refractory castables is to act as a filler. Indeed, it does not dissolve enough to enter into the katoite structure in significant extent and most of it remains unreacted. Once properly dispersed, microsilia fills the voids between the coarser particles, releasing the entrapped water and increasing the packing density. This improvement in the distribution of the hydration products results in an improvement of the structure of the castable, providing it more density. Then the material becomes stronger after it has hardened. On the other hand, the formation by a dissolution precipitation process of calcium aluminate hydrates,  $\text{Al}(\text{OH})_3$  (gibbsite), amorphous  $\text{Al}(\text{OH})_x$  and amorphous calcium silicate and calcium aluminosilicate hydrates (C–S–H and C–S–A–H phases), from the aqueous phase, may enhance the mechanical properties of the setting samples.

By examining the results obtained Tables 4–6, it can be appreciated that for a  $\text{CaO}/\text{Al}_2\text{O}_3$  ratio  $\leq 3$  in the initial chemical composition, calcium hydroxide does not precipitate at temperatures lower than  $90^\circ\text{C}$ . This fact is of great importance from a technological point of view since the absence of calcium hydroxide could avoid the formation of free CaO in the critical stages of heating and setting up of castables.

## 5. Conclusions

The main hydrates found among the reaction products upon mixing water and amorphous silica with  $\text{Ca}_3\text{Al}_2\text{O}_6$ ,  $\text{Ca}_{12}\text{Al}_{14}\text{O}_{33}$  and  $\text{CaAl}_2\text{O}_4$  at 40, 65 and  $95^\circ\text{C}$  are katoite ( $\text{Ca}_3\text{Al}_2(\text{SiO}_4)_{3-x}(\text{OH})_{4x}$ ), gibbsite,  $\text{Al}(\text{OH})_3$ , amorphous phases like  $\text{Al}(\text{OH})_x$  and amorphous calcium silicate and calcium aluminosilicate hydrate phases (C–S–H and C–S–A–H).

The stoichiometry of katoite,  $\text{Ca}_3\text{Al}_2(\text{SiO}_4)_{3-x}(\text{OH})_{4x}$ , main hydrated crystalline product, according to Rietveld refinement of X-ray and ND data, and TEM ranges between  $0 \leq (3-x) \leq 0.334$  and this value increases with temperature. It has been shown that temperature plays an important role on the mechanism and formation rate of

hydrated phases. Also it influences the extent of Si substitution in katoite.

In refractory castables technology, most of the amorphous silica which does not enter the katoite host structure, acts as filler. The microsilica fills the voids between the coarser particles increasing the packing density. This improvement in the distribution of products results in an improvement of the structure of the castable, providing it more density.

In the conditions of the experiment,  $T < 90^\circ\text{C}$  and water/solids = 2, none of the samples with silica content lower than 22 mol% exhibited the crystalline phase  $\text{Ca}_2\text{Al}_2\text{SiO}_7 \cdot 8\text{H}_2\text{O}$ .

### Acknowledgments

This research was partially supported by CICYT under the projects MAT-2000-0941 and MAT2003-08331-C02-01. The ND data were acquired at the SINQ (Swiss Spallation Neutron Source-Paul Scherrer Institute Villigen, Switzerland) with the allocation beam time for experiment number II/025-18. We thank Dr. D. Sheptyakov for the experimental assistance in collecting the ND data.

### References

- [1] W.E. Lee, W. Viera, S. Zang, K. Ghanbari Ahai, H. Sarpoolaky, C. Parr, *Int. Mater. Rev.* 46 (3) (2001) 145–167.
- [2] J.M. Rivas Mercury, A.H. de Aza, X. Turrillas, P. Pena, *Bol. Soc. Esp. Ceram.* V 42 (5) (2003) 269–276.
- [3] J.M. Rivas Mercury, A.H. de Aza, X. Turrillas, P. Pena, *Bol. Soc. Esp. Ceram.* V 42 (6) (2003) 361–368.
- [4] J. Ding, Y. Fu, J.J. Beaudoin, *Adv. Cem. Res.* 7 (28) (1995) 171–178.
- [5] J. Ding, Y. Fu, J.J. Beaudoin, *Cem. Concr. Res.* 25 (6) (1995) 1311–1319.
- [6] C. Cohen-Addad, P. Ducros, *Acta Crystallogr.* 23 (1967) 220–230.
- [7] T.G. Jappy, F.P. Glasser, *Adv. Cement Res.* 4 (1) (1991/92) 1–8.
- [8] B. Myhre, American Ceramic Society 30th Annual Refractory Symposium, St. Louis, MS, March 1994.
- [9] P.S. de Silva, F.P. Glasser, *Cem. Concr. Res.* 23 (1993) 627–639.
- [10] D. Damidot, F.P. Glasser, *Cem. Concr. Res.* 25 (1) (1995) 22–28.
- [11] S. Kobayashi, T. Shoh, *Mineral J.* 11 (1983) 331–343.
- [12] J.M. Rivas Mercury, A.H. De Aza, X. Turrillas, P. Pena, *J. Solid State Chem.* 177 (2004) 866–874.
- [13] J.M. Rivas Mercury, A.H. De Aza, P. Pena, *J. Eur. Ceram. Soc.* 25 (2005) 3269–3279.
- [14] H. Saalfeld, M. Weed, *Z. Cristal., Kristallg.* 139 (1974) 129–135.
- [15] G.A. Lager, T. Armbruster, J. Faber, *Am. Mineral.* 72 (1987) 756–765.
- [16] C.R. Hubbard, H.E. Swanson, F.A. Mauer, *J. Appl. Crystallogr.* 8 (1975) 45.
- [17] G.S. Bauer, *Nucl. Instrum. Methods B* 139 (1–4) (1998) 65–71.
- [18] P. Fisher, et al., *Physica B* 276–278 (2000) 146–147.
- [19] J. Rodriguez Carvajal, Short reference guide of the program FULLPROF 2000 version 2001, Lab. Leon Brillouin (CEA CNRS), 2001.
- [20] OriginLab Corporation, Northampton, MA, 01060, USA. Program Origin Version 5.0 (1999), [www.OriginLab.com](http://www.OriginLab.com)
- [21] L.B. McCusker, R.B. Von Dreele, D.E. Cox, D. Louer, P. Scardi, *J. Appl. Crystallogr.* 32 (1999) 36–50.
- [22] L.W. Finger, D.E. Cox, A.P. Jephcoat, *J. Appl. Crystallogr.* 27 (1994) 892–900.
- [23] G.A. Lager, T. Armbruster, F.J. Rotella, G.R. Rossman, *Am. Mineral.* 74 (1989) 840–851.
- [24] R. Weiss, D. Grandjean, *Acta Crystallogr.* 17 (1964) 1329–1330.
- [25] W. Dennis, J. Foreman Jr., *Chem. Phys.* 48 (7) (1968) 3037–3041.
- [26] H. Sawada, *J. Solid State Chem.* 142 (2,1) (1999) 273–278.
- [27] ICSD. <http://www.icsdweb.fiz-karlsruhe.de>. Fachinformationszentrum, Karlsruhe, Germany, 2005.
- [28] G.P. Kostikova, P. Kostikov, *Inorg. Mater.* 29 (1993) 1005–1006.
- [29] H.M. Rietveld, *J. Appl. Crystallogr.* 2 (1969) 65–71.
- [30] R.A. Young, *The Rietveld Method*, Oxford University Press, Oxford, 1993.
- [31] A.C. Larson, R.B. Von Dreele, Los Alamos National Laboratory Report No. LA-UR-86-748, 1994.
- [32] S. Rashid, X. Turrillas, *Thermochim. Acta* 302 (1–2) (1997) 25–34.
- [33] T.R. Jensen, A.N. Christensen, J.C. Hanson, *Cem. Concr. Res.* 35 (2005) 2300–2309.
- [34] A.N. Christensen, T.R. Jensen, N.V.Y. Scarlett, I.C. Madsen, J.C. Hanson, *J. Am. Ceram. Soc.* 87 (2004) 1488–1493.
- [35] J.M. Rivas Mercury, Ph.D. Thesis, Autonomous University of Madrid, November 2004.
- [36] S.H. Chan, *Geothermica* 18 (1–2) (1989) 49–56.
- [37] L. Vegard, H. Dale, *Z. Kristallogr.* 67 (1928) 148–162.